

## Electronic Supplementary Information

### Two organic-inorganic hybrid 1-D and 3-D polyoxotungstates constructed from hexa-Cu<sup>II</sup> substituted sandwich-type arsenotungstate units

Junwei Zhao,\*<sup>a</sup> Dongying Shi,<sup>a</sup> Lijuan Chen,<sup>ab</sup> Xiaomeng Cai,<sup>a</sup> Zhiqiao Wang,<sup>a</sup> Pengtao Ma,<sup>a</sup> Jingping Wang,<sup>a</sup> and Jingyang Niu\*<sup>a</sup>

<sup>a</sup> Institute of Molecular and Crystal Engineering, College of Chemistry and Chemical Engineering, Henan University, Kaifeng, Henan 475004, P. R. China. E-mail: zhaojunwei@henu.edu.cn, jyniu@henu.edu.cn, Fax: (+86) 3783886876

<sup>b</sup> Basic Experiment Teaching Center, Henan University, Kaifeng, Henan 475004 P. R. China

**Fig. S1** IR spectra of **1** and **2**.

**Fig. S2** (a) The PXRD pattern of **1** before (Experimental1) and after (Experimental2) after the photocatalytic degradations of RhB and its calculated pattern based on the single-crystal structural analysis. (b) The PXRD pattern of **2** before (Experimental1) and after (Experimental2) after the photocatalytic degradations of RhB and its calculated pattern based on the single-crystal structural analysis.

**Fig. S3** The packing arrangement of 1-D chains in **1**.

**Fig. S4** IR spectrum of Na<sub>8</sub>[A- $\alpha$ -HAsW<sub>9</sub>O<sub>34</sub>]·11H<sub>2</sub>O.

**Fig. S5** TGA curves of **1** and **2**.

**Fig. S6** Temperature evolution of the inverse magnetic susceptibility  $\chi_M^{-1}$  for **1** between 2 and 300 K. The solid line was generated from the best fit by the Curie-Weiss expression.

**Fig. S7** Temperature evolution of the inverse magnetic susceptibility  $\chi_M^{-1}$  for **2** between 2 and 300 K. The solid line was generated from the best fit by the Curie-Weiss expression.

**Fig. S8** UV-visible absorption spectral changes for the RhB solutions (a), in the presence of **1** (b), in the presence of **2** (c), in the presence of Na<sub>8</sub>[A- $\alpha$ -HAsW<sub>9</sub>O<sub>34</sub>]·11H<sub>2</sub>O (d) in darkness.

**Fig. S9** UV-visible absorption spectral changes for the RhB solutions at various irradiation times in the presence of Na<sub>8</sub>[A- $\alpha$ -HAsW<sub>9</sub>O<sub>34</sub>]·11H<sub>2</sub>O. Inset: the conversion of RhB ( $K$ ) with reaction time ( $t$ ).

**Fig. S10** The representations of (a) the coplanar belt-like Cu<sub>6</sub> clusters, (b) the hexagonal Cu<sub>6</sub> clusters, (c) the coplanar Cu<sub>8</sub> clusters; (d) the rhombus Cu<sub>4</sub> clusters and (e) the triangle Cu<sub>6</sub> clusters.

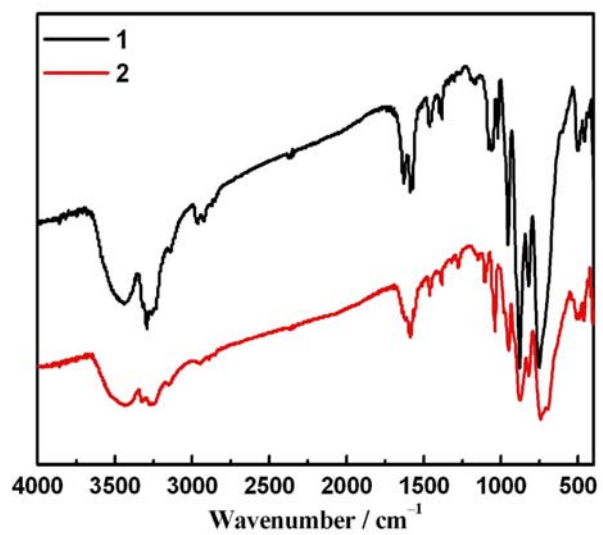


**Fig. S1** IR spectra of **1** and **2**.

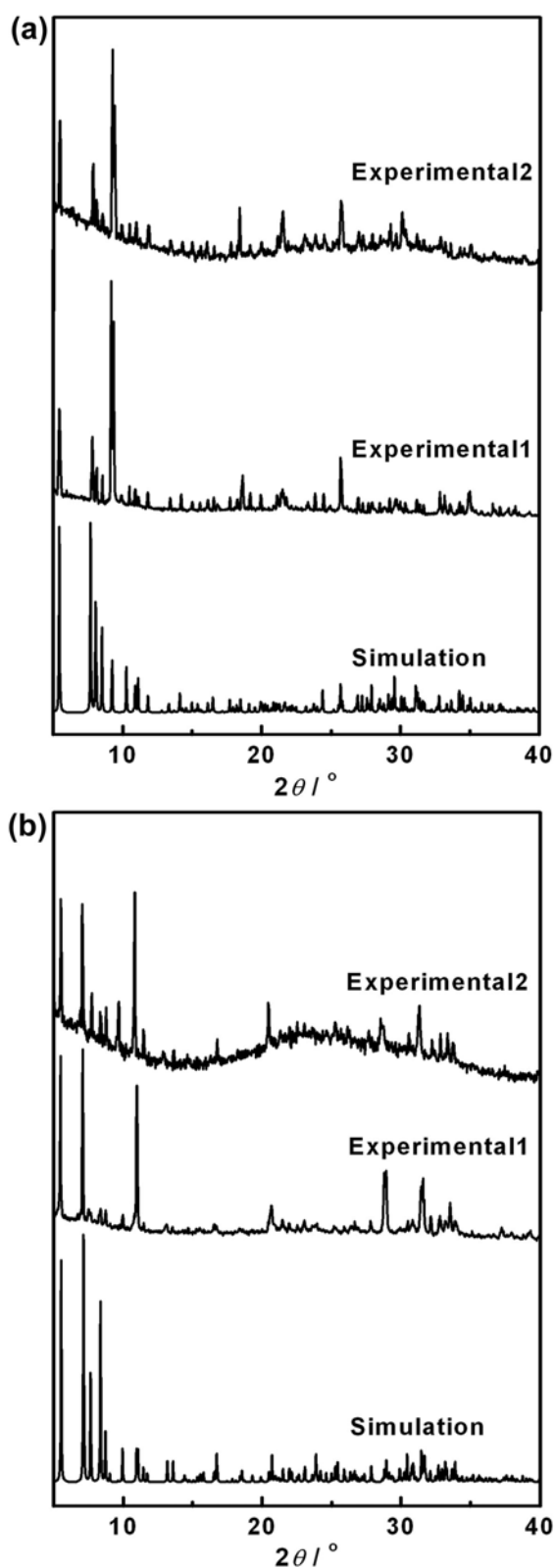


**Fig. S2** (a) The PXRD pattern of **1** before (Experimental1) and after (Experimental2) after the photocatalytic degradations of RhB and its calculated pattern based on the single-crystal structural analysis. (b) The PXRD pattern of **2** before (Experimental1) and after (Experimental2) after the photocatalytic degradations of RhB and its calculated pattern based on the single-crystal structural analysis.

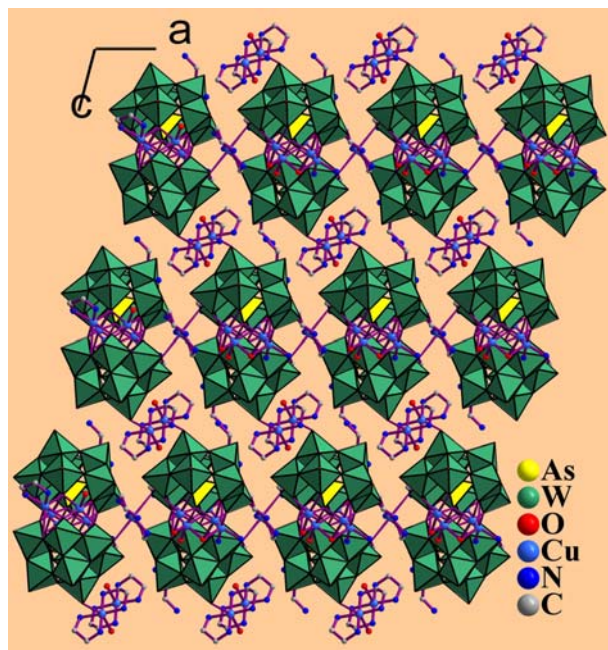


Fig. S3 The packing arrangement of 1D chains in 1.

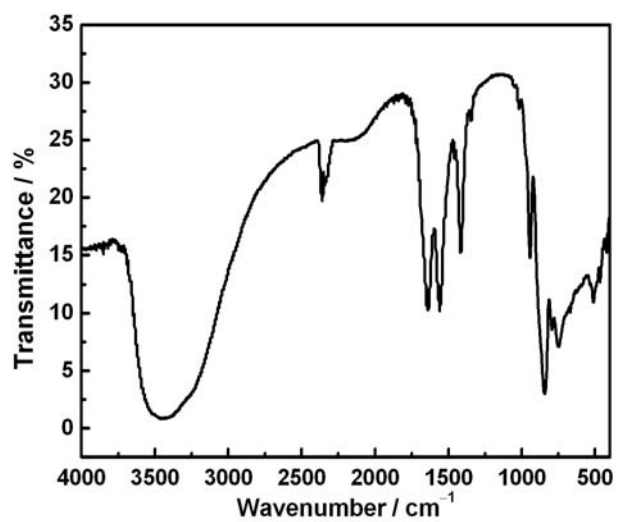


Fig. S4 IR spectrum of Na<sub>8</sub>[A- $\alpha$ -HAsW<sub>9</sub>O<sub>34</sub>]·11H<sub>2</sub>O.

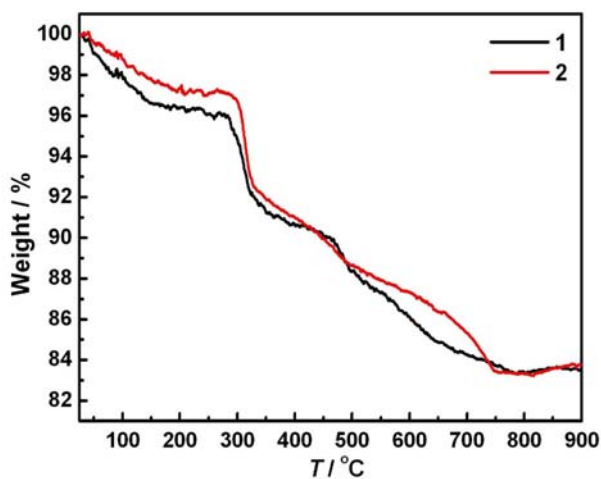


Fig. S5 TGA curves of 1 and 2.

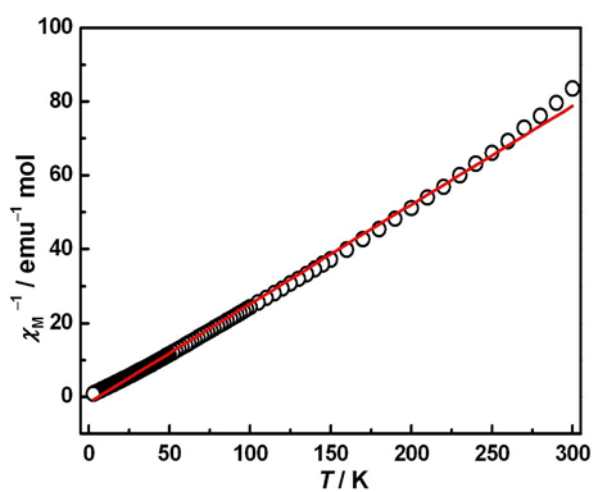


Fig. S6 Temperature evolution of the inverse magnetic susceptibility  $\chi_M^{-1}$  for 1 between 2 and 300 K. The solid line was generated from the best fit by the Curie-Weiss expression.

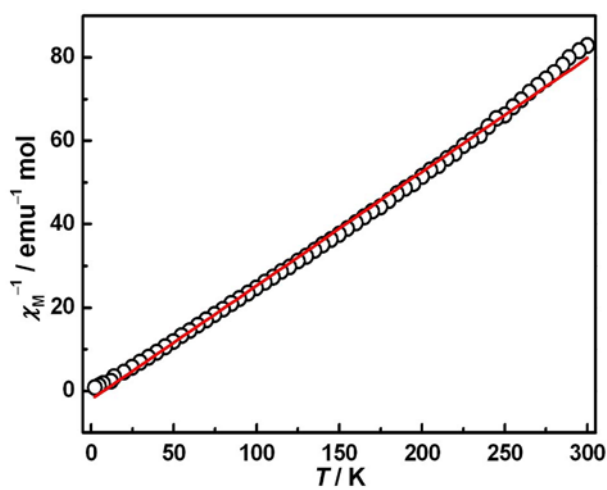
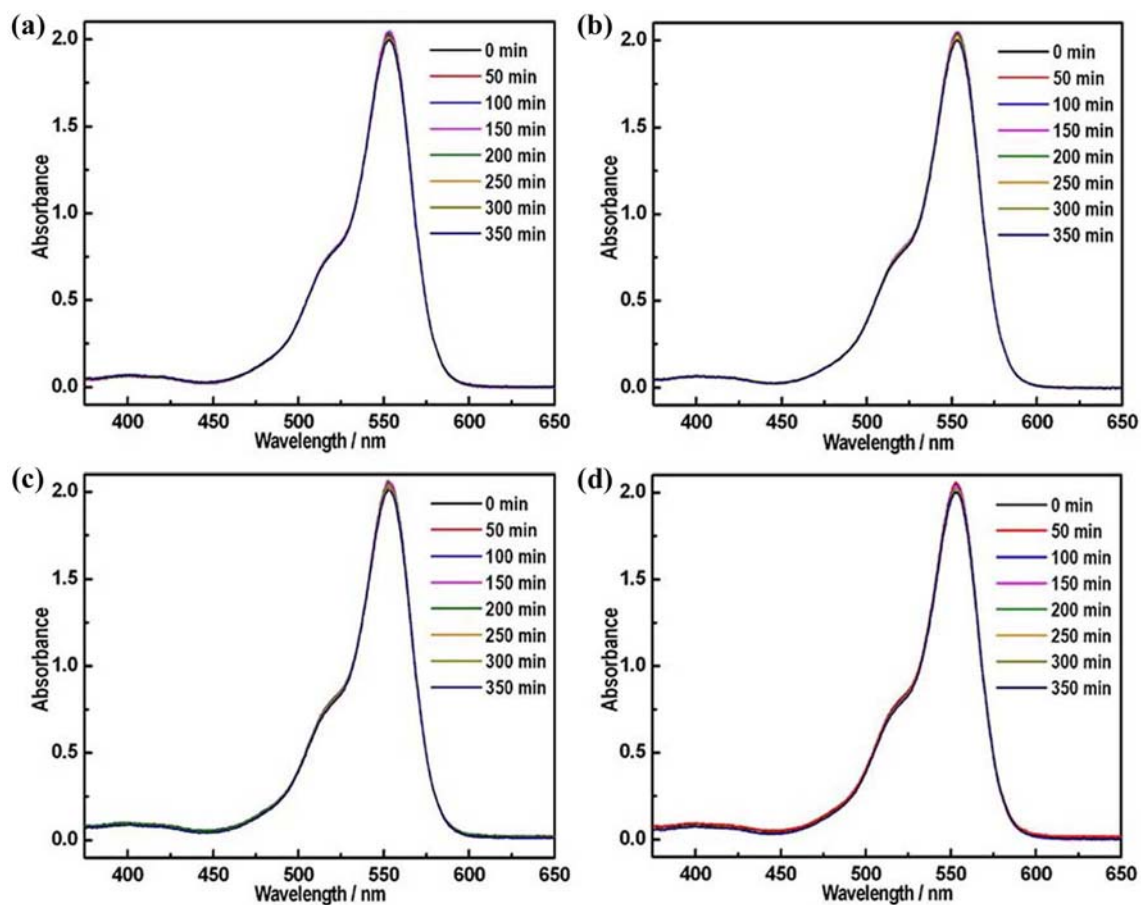
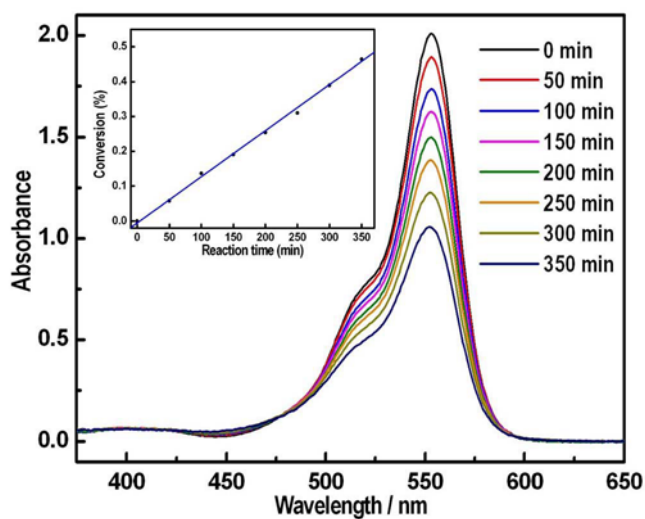


Fig. S7 Temperature evolution of the inverse magnetic susceptibility  $\chi_M^{-1}$  for 2 between 2 and 300 K. The solid line was generated from the best fit by the Curie-Weiss expression.



**Fig. S8** UV-visible absorption spectral changes for the RhB solutions (a), in the presence of **1** (b), in the presence of **2** (c), in the presence of  $\text{Na}_8[\text{A-}\alpha\text{-HAsW}_9\text{O}_{34}] \cdot 11\text{H}_2\text{O}$  (d) in darkness.



**Fig. S9** UV-visible absorption spectral changes for the RhB solutions at various irradiation times in the presence of  $\text{Na}_8[\text{A-}\alpha\text{-HAsW}_9\text{O}_{34}] \cdot 11\text{H}_2\text{O}$ . Inset: the conversion of RhB ( $K$ ) with reaction time ( $t$ ).

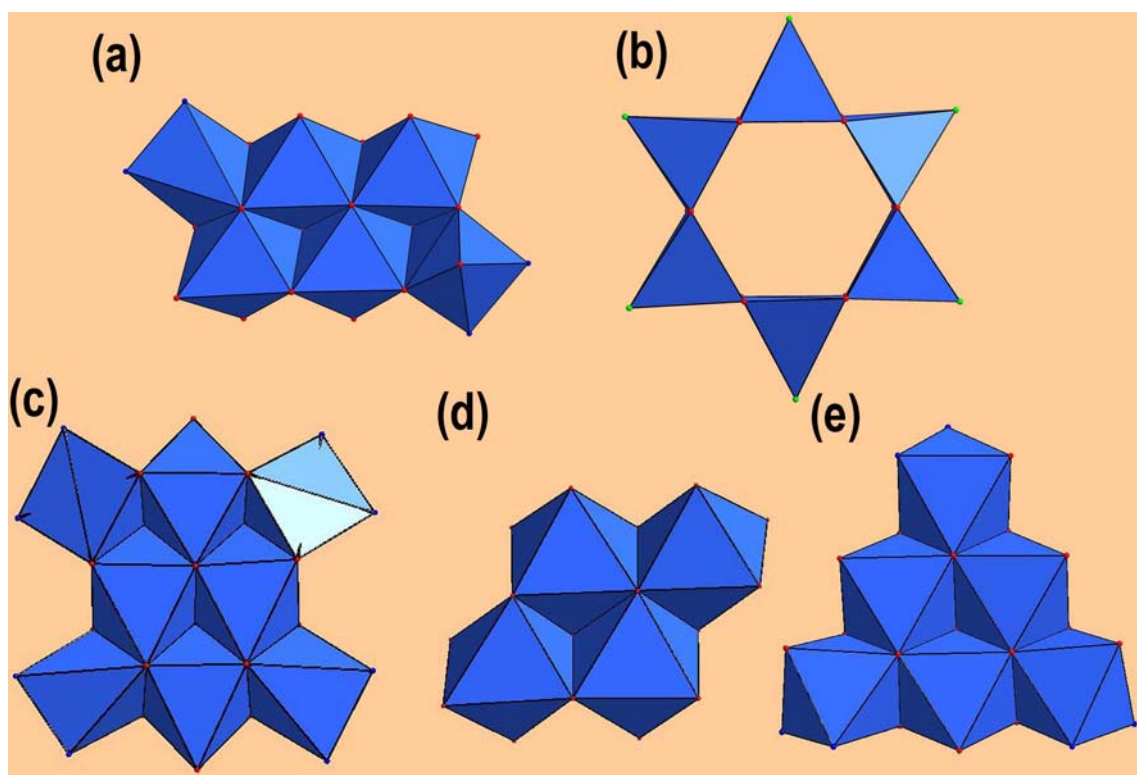


**Fig. S10** The representations of (a) the coplanar belt-like  $\text{Cu}_6$  clusters, (b) the hexagonal  $\text{Cu}_6$  clusters, (c) the coplanar  $\text{Cu}_8$  clusters; (d) the rhombus  $\text{Cu}_4$  clusters and (e) the triangle  $\text{Cu}_6$  clusters.